JGE (Jurnal Geofisika Eksplorasi)
Vol. 11 No. 03, November 2025 (227-239) https://doi.org/10.23960/jge.v11i3.505

PHASE TENSOR AND MODELING OF MAGNETOTELLURIC DATA TO DETECT FAULT STRUCTURES IN ETHERIDGE AREA

ANALISIS TENSOR FASE DAN PEMODELAN DATA MAGNETOTELLURIK UNTUK MEMPERKIRAKAN STRUKTUR SESAR DI DAERAH ETHERIDGE

Deo Rizqiqa Fawwaz[1*], Selvi Misnia Irawati [2] , Purwaditya Nugraha [3]

[1,2,3]Geophysical Engineering Study Program, Sumatra Institute of Technology; Jl. Terusan Ryacudu, Desa Way Huwi, Jati Agung, Lampung Selatan, Lampung 35365

Received: 2025, October 23rd
Accepted: 2025, January 06th

Keywords:
Etheridge;
Fault Structure;
Magnetotellurics;
Phase Tensor Analysis;
2D Inversion.

Correspondent Email:
deorizqiqa97@gmail.com

How to cite this article :
Fawwaz, D.R., Irawati, S.M., & Nugraha, P. (2025). Phase Tensor and Modeling of Magnetotelluric Data to Detect Fault Structures in The Etheridge Area. *JGE (Jurnal Geofisika Eksplorasi)*, 11(03), 227-239.

Abstract. This study aims to identify subsurface fault structures in the Etheridge region, Queensland, Australia, using the magnetotelluric (MT) method. The data used consists of 21 secondary MT points from Geoscience Australia. Phase tensor analysis shows the dominance of a 2D structure with a geophysical direction of N175°E, which is then used as the basis for 2D inversion modeling using the Non-Linear Conjugate Gradient (NLCG) algorithm to a depth of ±2.2 km. The modeling results show a low-to-medium resistivity zone (<500 Ωm) interpreted as a fault zone and fluid-saturated rock, as well as high resistivity (>1500 Ωm) representing igneous-metamorphic rock. The main structures identified are the Delaney Fault and the Palmerville Fault. The novelty of this study lies in the mapping of regional fault continuity based on phase tensor integration and 2D inversion, which provides a better understanding of tectonic control and potential fluid flow pathways in the Etheridge area.

Abstrak. *Studi ini bertujuan untuk mengidentifikasi struktur sesar bawah permukaan di wilayah Etheridge, Queensland, Australia, menggunakan metode magnetotellurik (MT). Data yang digunakan terdiri dari 21 titik MT sekunder dari Geoscience Australia. Analisis tensor fase menunjukkan dominasi struktur 2D dengan arah geofisika N175°E, yang kemudian digunakan sebagai dasar untuk pemodelan inversi 2D menggunakan algoritma Non-Linear Conjugate Gradient (NLCG) hingga kedalaman ±2,2 km. Hasil pemodelan menunjukkan zona resistivitas rendah hingga sedang (<500 Ωm) yang diinterpretasikan sebagai zona sesar dan batuan jenuh fluida, serta resistivitas tinggi (>1500 Ωm) yang mewakili batuan beku-metamorf. Struktur utama yang diidentifikasi adalah Sesar Delaney dan Sesar Palmerville. Keunikan studi ini terletak pada pemetaan kontinuitas*

sesar regional berdasarkan integrasi tensor fase dan inversi 2D, yang memberikan pemahaman yang lebih baik tentang kontrol tektonik dan jalur aliran fluida potensial di wilayah Etheridge.

1. INTRODUCTION

Australia is characterized by complex lithospheric architecture and tectonic activity reflected in large-scale subsurface resistivity patterns (Kirkby et al., 2020). In the Etheridge region of Queensland, historical seismic activity is closely related to the Delaney Fault, which has a steep to subvertical geometry, developed in the upper crust at depths of approximately 5–15 km, and acts as a fracture and fluid pathway manifested as a low to medium resistivity zone in magnetotelluric data (Withnall & Blake, 2012; Jiang et al., 2020). In contrast, the Palmerville Fault, a large regional structure that borders the Etheridge and Tasmanides Provinces, has a steep geometry with structural roots extending over 30 km, even reaching the lower crust, resulting in more continuous deep resistivity anomalies than local faults (Korsch et al., 2012). Mapping fault structures is crucial due to their association with seismic activity and their role as fluid pathways that control economic potential such as mineralization and aquifers (Zhang & Nie, 2024). Therefore, this study uses the magnetotelluric (MT) method to identify subsurface fault structures through resistivity distribution, which begins with phase tensor analysis because of its resistance to galvanic distortion and its ability to determine the dimensions of the structure and the dominant conductivity direction as an indicator of electrical discontinuity that represents the presence of faults (Tietze et al., 2024; Ostersen, 2024).

2. LITERATURE REVIEW

This research was conducted in the Etheridge region, Queensland, Australia (approximately 18° 33' S, 141° 52' E). The geology of this region is characterized by complex crustal architecture controlled by large-scale electrical conductivity structures in the lithosphere (Korsch et al., 2012). The regional geological map of the study area is shown in **Figure 1**.

The Etheridge region of northern Queensland lies in the transition zone between the Etheridge Province and the Tasmanides orogenic belt, which records repeated deformation from the Proterozoic to Phanerozoic. This regional tectonic framework is characterized by steep-to-near-vertical regional faults that potentially extend into the middle-lower crust, making them relevant for interpreting dip direction, depth range, and structural continuity in magnetotelluric (MT) resistivity models (Withnall & Blake, 2012). Geologically, the region is composed of intrusively cut Proterozoic to Paleozoic rocks, overlain by Mesozoic and Cenozoic–Quaternary sediments. These age and lithological variations control subsurface resistivity contrasts, such that low resistivity anomalies can be attributed to fault zones or alteration, while high resistivity anomalies reflect massive igneous–metamorphic rocks. Therefore, MT resistivity sections can be directly compared with published regional geological maps and sections to validate fault geometry and their association with rock units (Terrex, 2007).

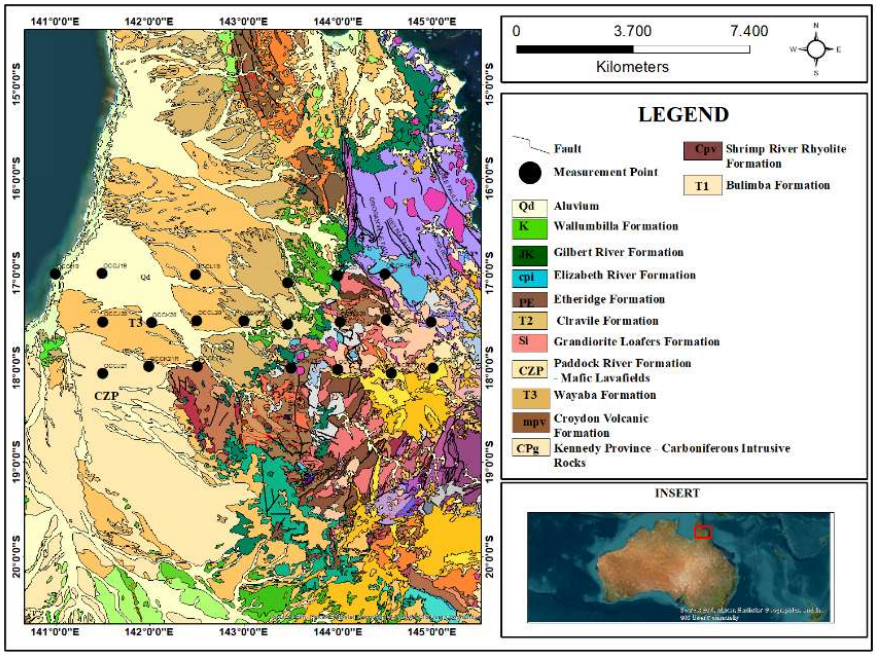

Figure 1. Regional Geological Map (Withnall & Blake, 2012).

3. RESEARCH METHODS

3.1. Data Location and Research

This research was conducted in the Etheridge region, Queensland, Australia. Geographically, this region is located at latitude 142°52.0' E and longitude 18°330' S. This study uses secondary data in *edi format obtained from the official Openei website published by the Australian Government Geosciences, with a total of 21 measurement points. The area covered by this study is 75,553 km^2, with a distance between measurement points of 50 to 56 km. The design of the research area acquisition can be seen in (**Figure 2**).

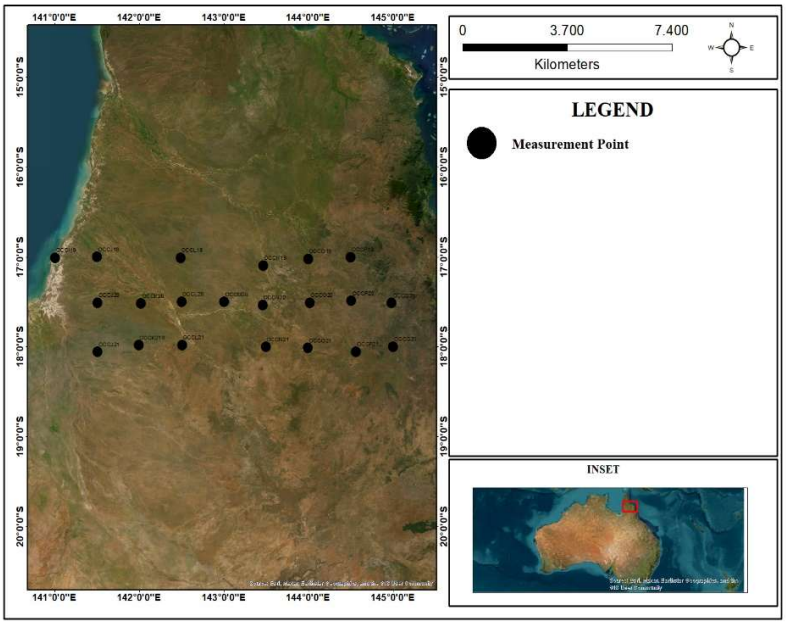

Figure 2. Acquisition design map.

3.2. Magnetotelluric Method

This study uses passive Magnetotelluric (MT) geophysical methods to map subsurface rock resistivity. The analysis is divided into two stages: first, phase tensor analysis is performed to correct galvanic distortion and determine the dimensions of the dominant structure (2D) and the direction of geoelectric strike (N85 ° E). Second, 2D modeling is performed using NLCG inversion (a combination of TE and TM modes). The result is a 2D resistivity cross section that successfully identifies the suspected main fault structure (Delaney Fault) and other structural extensions (Palmerville Structure) characterized by sharp resistivity contrasts.

3.2.1. Magnetotelluric Signal

Method is used to map the resistivity of subsurface rocks, which reflects rock type, fluid content, and temperature (Robertson, 2020). MT signals originate from low frequencies (<1 Hz) resulting from the interaction of the solar wind with the magnetosphere and high frequencies (>1 Hz) from lightning (Tietze et al., 2024). By analyzing variations in the Earth's magnetic field, MT measures secondary magnetic fields to interpret geological structures, but requires modern processing such as phase tensor analysis to correct distortions and obtain reliable results (Ostersen, 2024).

3.2.2. Basic Principles of EM Method Propagation on Magnetotelluric Data

The magnetotelluric (MT) method is based on Maxwell's equations relating the electric (E) and magnetic (H) fields in the Earth (Robertson, 2020). Assuming a homogeneous, isotropic, and quasi-static medium (neglecting displacement currents), these equations simplify to a frequency-dependent diffusion equation that depends on the rock conductivity (σ) and the angular frequency (ω) of the MT signal (Kirkby et al., 2020; Tietze et al., 2024).

3.2.3. Phase Tensor Analysis

Phase tensor analysis is a complex number phase obtained based on the comparison value of the real (X) and imaginary (Y) part (Maharani et al., 2023). Then, the complex matrix equation is obtained from the separation of the complex impedance tensor into a real impedance tensor (X) and an imaginary impedance tensor (Y) in the following equation:

$$Z = X + iY \quad (1)$$

$$\emptyset = X^{-1}Y = \begin{bmatrix} \emptyset_{xx} & \emptyset_{xy} \\ \emptyset_{yx} & \emptyset_{yy} \end{bmatrix} \quad (2)$$

Z= Impedance tensor
X= Real numbers
Y= Imaginary numbers
$\emptyset$= Phase tensor

From equation (2) above, X (-1) is the inverse of the tensor value *(X)* and ϕ is a real number. The relationship between the observed phase tensor and impedance tensor can be written in the following equation:

$$\begin{bmatrix} \emptyset_{11} & \emptyset_{12} \\ \emptyset_{21} & \emptyset_{22} \end{bmatrix} = \frac{1}{\det(X)} \begin{bmatrix} X_{22}Y_{11} - X_{12}Y_{21} & X_{22}Y_{12} - X_{12}Y_{22} \\ X_{21}Y_{21} - X_{21}Y_{11} & X_{11}Y_{22} - X_{21}Y_{12} \end{bmatrix} \quad (3)$$

The phase tensor can be depicted as an oval (ellipse) with a specific angle. This angle is very important because it indicates the degree of heterogeneity, or differences in electrical conductivity, in the subsurface rock.

3.2.4. Geoelectrical Strike Analysis

Geological directional analysis in the magnetotelluric (MT) method is a fundamental step in determining the orientation of dominant structures, such as faults, using **the phase tensor** and visualization through a principal axis rose diagram (Simpson & Bahr, 2005; Pahri, 2023; Murdani & Sarkowi, 2019). Determining this direction is important for validating the structure's dimensions and providing precise rotation angles before 2D inversion modeling. However, this method has a 90° ambiguity, so the results of the MT strike analysis need to be combined with regional geological data to ensure accurate structural interpretation (Pahri, 2023).

3.2.5. MT Data Dimensionality

Dimensionality analysis is essential before modeling to classify subsurface media into 1D, 2D, or 3D (Tietze, 2024). 1D media only vary with depth, while 2D media vary laterally and vertically, usually assumed to be linear fractures (Ostersen, 2024). In the 2D case, measurements parallel (TE) or perpendicular (TM) to the

geoelectric strike simplify the impedance matrix into two independent components for 2D inversion modeling (Robertson, 2020).

3.2.6. 2D Modeling of Magnetotelluric (MT) Data

MT modeling to map subsurface structures is carried out by 2D inversion using the Non-Linear Conjugate Gradient (NLCG) algorithm, which produces a resistivity model according to measured data and remains geologically valid, with fault identification depending on TE and TM data adjusted based on the Phase Tensor (Robertson, 2020; Ostersen, 2024; Jiang et al., 2024). The model inversion equation can be written as follows:

$$d = f(m) + e \quad (4)$$

NLCG (*Non-Linear Conjugate Gradient*) simplifies modeling by smoothing MT data to minimize the objective function (ψ) related to the model resistivity (m) while taking into account measurement error (e). Model solution to simplify the objective function *(ψ)* can be written as the following equation:

$$\psi(m) = \left(d - F(m)\right)^T V^{-1}\left(d - F(m)\right) + \tau m^T L^T L m \quad (5)$$

$\psi(m)$ = Inverse objective function
d = MT observation data
$F(m)$ = Synthetic data resulting from modeling from the model m
V^{-1} = Weight matrix/ inverse covariance of data errors
m = Model parameters
$.^T$ = Regularization Parameter

3.3. Flow diagram

This workflow illustrates the stages of Magnetotelluric (MT) data analysis from initial preparation to final interpretation. The study begins with a literature review and compilation of regional geological information. MT data in .edi format are evaluated using phase tensor analysis to determine dimensionality and the dominant structural direction, followed by data rotation and quality control procedures. The processed data are then sliced along the survey lines and subjected to two-dimensional inversion to produce resistivity cross-sections, which are finally interpreted by integrating geological constraints and supporting data (Yulianti, 2020).

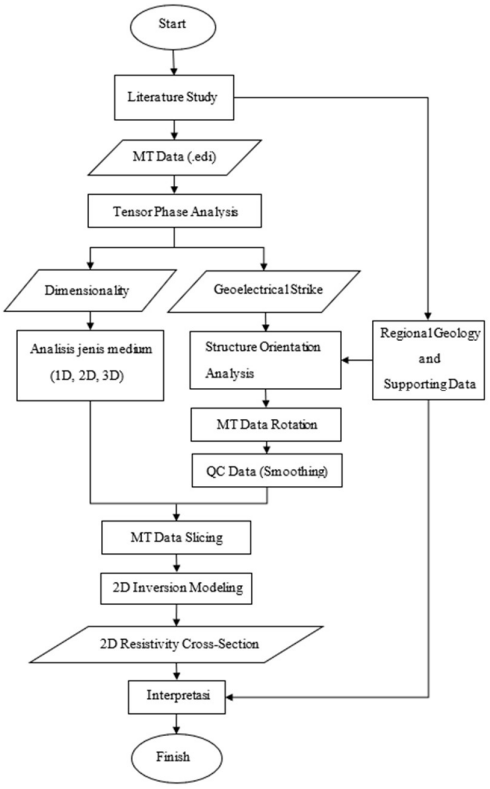

Figure 3. Flow diagram.

4. RESULTS AND DISCUSSION

4.1. MT data dimensionality

Through phase tensor analysis of Magnetotelluric (MT) data from 21 stations, we identified the dimensions and orientations of subsurface geological structures. Analysis of dip angle variations and rose diagrams were used to determine the dimensions of the structures (1D, 2D, or 3D) and the dominant direction of electric current (geoelectric direction). Phase tensor analysis was performed at low (10 s or 10−1Hz), medium (1000 s or 10−3Hz), and high (10000 s or 10−4Hz) periods. The phase tensor results of 21 MT for all periods are shown in **Figure 4**.

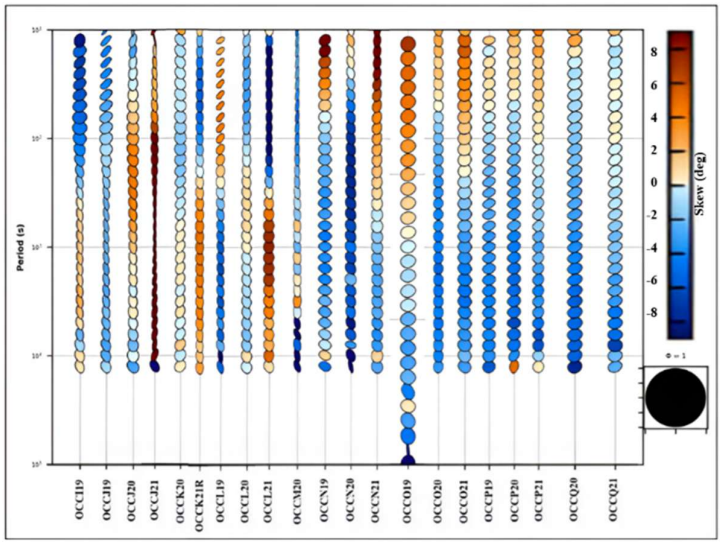

Figure 4. Phase tensor of 21 MT over the entire period.

Tensor phase analysis classifies media based on elliptical shape and tilt angle (β): 1D (circular, β≈0°), 2D (symmetric elliptical, −3°<β<3°), and 3D (asymmetric elliptical, β>3° or β<−3°). The results show 2D dominance throughout the entire period (10–10,000 s), which strengthens the decision for 2D modeling.

4.2. Geoelectrical strike from MT data

In this study, the determination of the geoelectric strike direction can be seen in the range of low, medium, and high periods. **Figure 5A** shows the plot of the geoelectric strike direction at a low period or 10 s (10^1 –10^2 s) with an orientation of N70 ° E. **Figure 5B** and **C** show the plot of the geoelectric strike direction at a medium period or 100–1,000 s (10^2 –10^3 s). **Figure 5D** shows the plot of the geoelectric strike direction at a high period or 10,000 s (10^4 – 10^5 s) with an orientation of N315 ° E.

Based on the phase tensor analysis (**Figure 6**), the initial geoelectrical strike direction is N85° E. This direction differs by 90° from the regional main fault direction (~N180 ° S) due to the 90° ambiguity. Therefore, an angular correction was performed, resulting in a structural direction of N175° E. The MT data were then rotated by 175°, which was successfully demonstrated by significant changes in the apparent resistivity curves of TE and TM modes (**Figure 7b**), while the phase curves remained unchanged, validating that the data rotation successfully addressed the galvanic distortion.

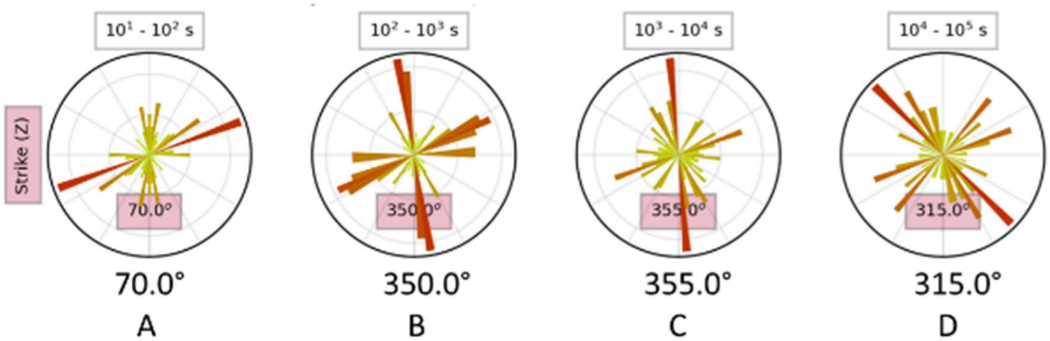

Figure 5. (A) Rose diagram during the low period (10^1 - 10^2 s). (B and C) Rose diagram during the middle period ($10^{2\ -\ 10^3}$ s and $10^{3\ -}$ 10^4s). (D) Rose diagram during the high period (10^4 -10^5 s).

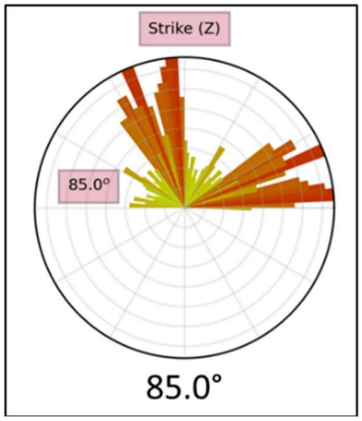

Figure 6. Rose chart for the entire period.

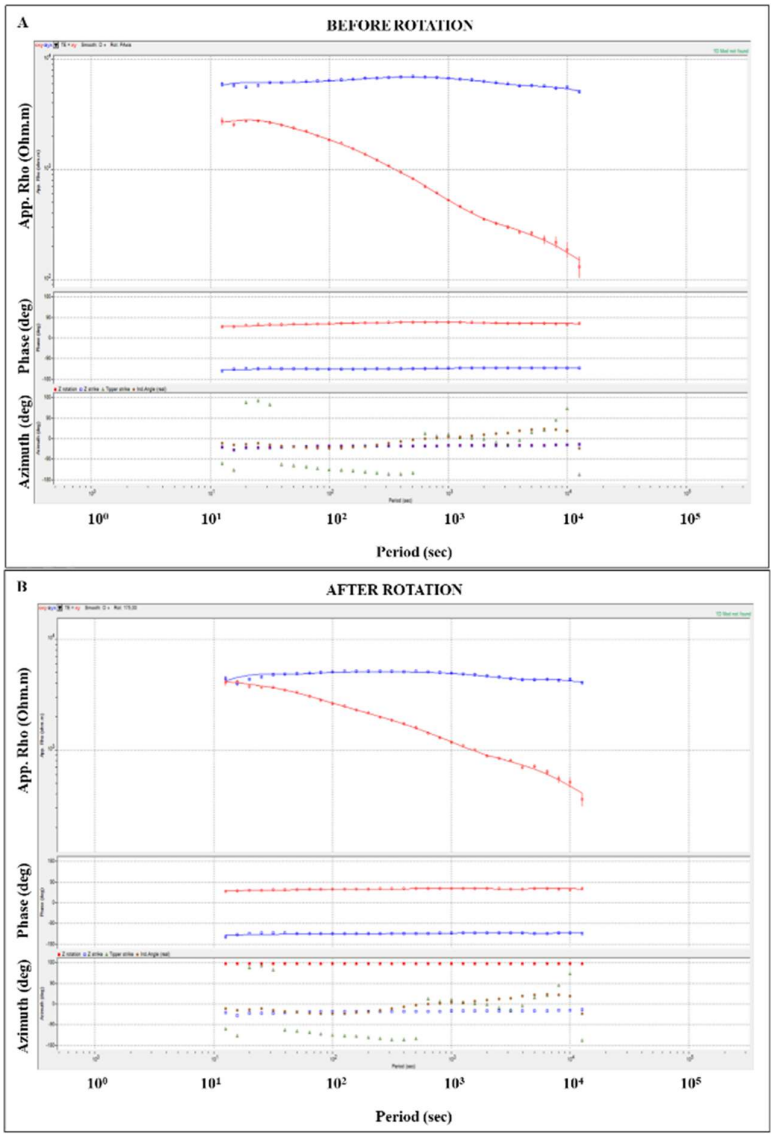

Figure 7. (A) MT data before rotation, (B) MT data after rotation.

4.3. 2D Modeling

2D modeling was performed using Nonlinear Conjugate Gradient (NLCG) inversion on MT data to obtain the subsurface resistivity distribution. This modeling used WinGlink software and involved 21 MT stations divided into 3 lines (as shown in **Figure 8**).

The initial MT modeling model (**Figure 9**) is assumed to be a homogeneous half-space with a resistivity of 1000 Ωm to minimize the initial bias. The grid network is enlarged 2-3 times for smooth results. The Non-Linear Conjugate Gradient (NLCG) inversion algorithm is used to minimize the minimum function and the influence of outlier data for an optimal solution. This inversion model combines Transverse Electric (TE) and Transverse Magnetic (TM) modes, where the TE mode excels in vertical (depth) details and the TM mode excels in lateral (horizontal) details, resulting in an accurate and comprehensive subsurface model.

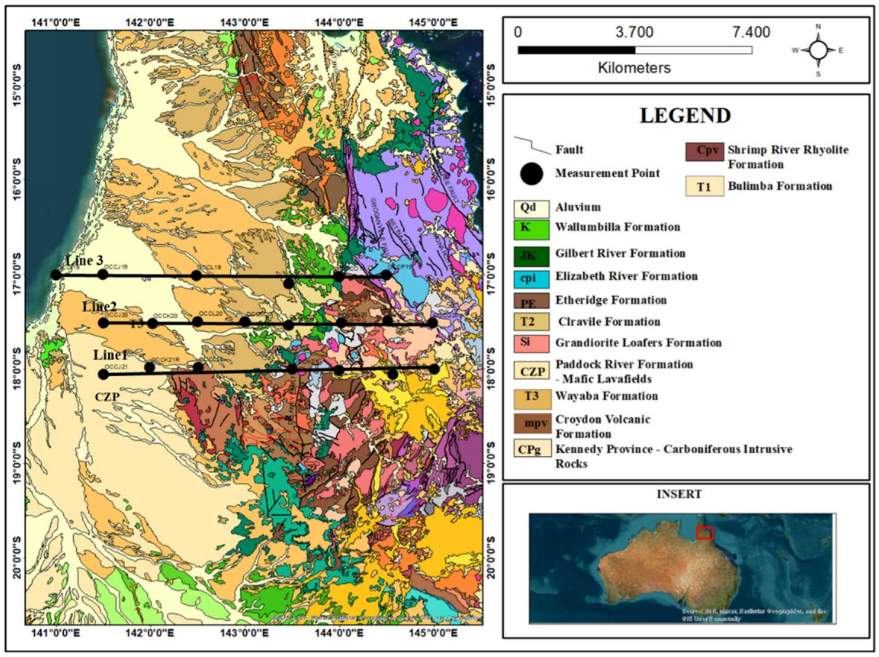

Figure 8. Mapping of slices at MT measurement points based on geological structures (Withnall & Blake, 2012).

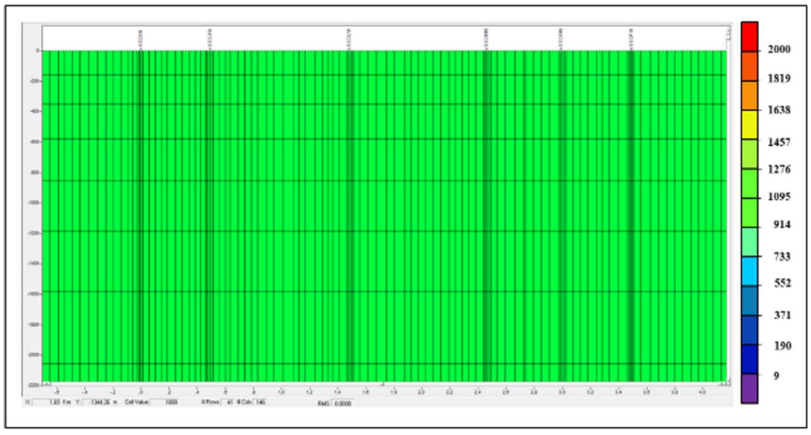

Figure 9. Initial 2D inversion model.

Table 1. Inversion parameters for each Line 1, 2, and 3.

Line 1	Line 2	Line 3
Alpha 1	Alpha 0.2	Alpha 0.5
Beta 2	Beta 1	Beta 1
Tau 1	Tau 7	Tau 7

Table 2. Testing the *Tau* value of each line.

Tau	RMS	Roughness	Tau	RMS	Roughness	Tau	RMS	Roughness
0.1	5.016837	71.7	0.1	4.63932	271.6	0.1	8.35645	133.9
0.3	5.063102	72.3	0.3	4.61538	310.1	0.3	7.16045	206.3
0.5	5.004649	91.3	0.5	4.69453	330	0.5	8.41273	340.4
0.7	5.003501	105.3	0.7	4.62659	302.8	0.7	7.55531	279.7
0.9	5.037843	92.3	0.9	4.67212	389.2	0.9	7.77779	261.3
1	4,972961	110.4	1	4.62338	367.6	1	7.68698	283.6
3	5.16648	106.6	3	4.85186	525	3	7.35733	540.7
5	5.236581	151.8	5	4.47316	707.9	5	7.21393	660.7
7	5.327248	193.8	7	4.25291	721.9	7	5.73148	481.6
9	5.380664	216.7	9	4.33236	757.5	9	6.44401	631.6

Inverse modeling uses different parameterizations per path (**Table 1**) to control the error and roughness to minimize the objective function through the tau *(τ) value* and the number of iterations. The initial resistivity homogeneity model of 1000 *Ω* m is set with 100 iterations. Optimal iterations are achieved when the RMS error is low and stable (**Figure 10**). The optimal τ value is determined based on the minimum and stable error and roughness. This process is also influenced by the Lagrange parameters: alpha *(α)* for horizontal refinement and beta *(β)* for vertical refinement, whose values vary for each model.

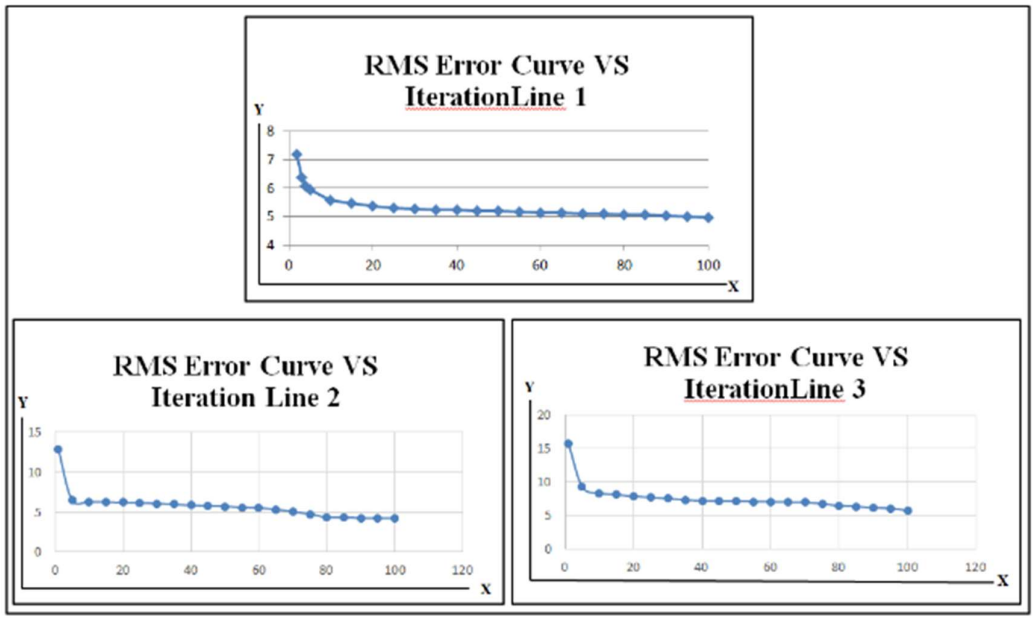

Figure 10. RMS error curve with iterations on rows 1, 2, and 3.

All Lines (1, 2, and 3) with the Y-axis being the RMS error value and the Y-axis being the number of iterations, show rapid convergence with a sharp decrease in the RMS error in the initial iterations, then stabilizing after approximately 80 iterations, validating that the Non-Linear Conjugate Gradient (NLCG) inversion process has achieved the optimal solution. The RMS error values in Line 1 show a good correlation between the observed data and the model, with most points below 5% (however, point OCCN21 reaches ~ 10.38%). Meanwhile, Line 2 and Line 3 also achieve high accuracy, as evidenced by the very low and stable minimum RMS error values of 4.252% (Line 2) and 5.731% (Line 3). This high accuracy (average RMS error below 7%) confirms that the resistivity model successfully represents the subsurface geological conditions realistically (**Table 2**).

Table 3. Rock resistivity in the research area (Tournerie, 2009).

No.	Rock	Resistivity (Ωm)
1	Clay	< 100
2	Sand	100 – 500
3	Quartz	500 – 1500
4	Basal	1500 – 10000
5	Granite	1500 – 100000

4.4. Line 1

2D modeling on line 1 (West–East), which consists of 7 MT stations (OCCJ21, OCCK21R, OCCL21, OCCN21, OCCO21, OCCP21, and OCCQ21) along 450 km to a depth of 2.2 km, aims to detect the Delaney Structure that stretches North–South. The results of 2D inversion (α 1, β 2, τ 1) produce a resistivity distribution of 9–2000 Ωm with an RMS error of 4,97% (**Figure 11**). This section crosses the Georgetown Inlier (rocks aged >1.5 billion years) and shows four main zones: C1 (<100 Ωm, water-saturated clay from the Paddock River/CZP Formation); 100–500 Ωm (water-saturated sandstone); 500–1500 Ω m (quartz from the Croydon Volcanic Formation/mpv); and R1 (>1500 Ω m, basalt from the Etheridge Formation/PE).

Traverse 1 results show an increase in high conductivity (C1) suspected to be a fault, where this conductive layer spreads south to a depth of 2.2 km; the fault structure is identified in the C1 layer due to the directional contrast and very low resistivity values. A small fault is suspected at station OCCK21R with an estimated depth of 500 meters, supported by resistivity contrast and geological maps, while the Delaney Fault is clearly identified at station OCCN21 suspected to be a small fault with a depth of 2,200 meters. The low to moderate resistivity contrast at station OCCQ21 is caused by differences in rock formations, not faults. Traverse 1 traverses six major rock formations: the Etheridge Formation (PE), the Paddock River Formation (CZP), the Grandiorite Loafers Formation (Si), the Croydon Volcanic Formation (mpv), the Sungai Udang Rhyolite Formation (Cpv), and the Claravile Formation (T2).

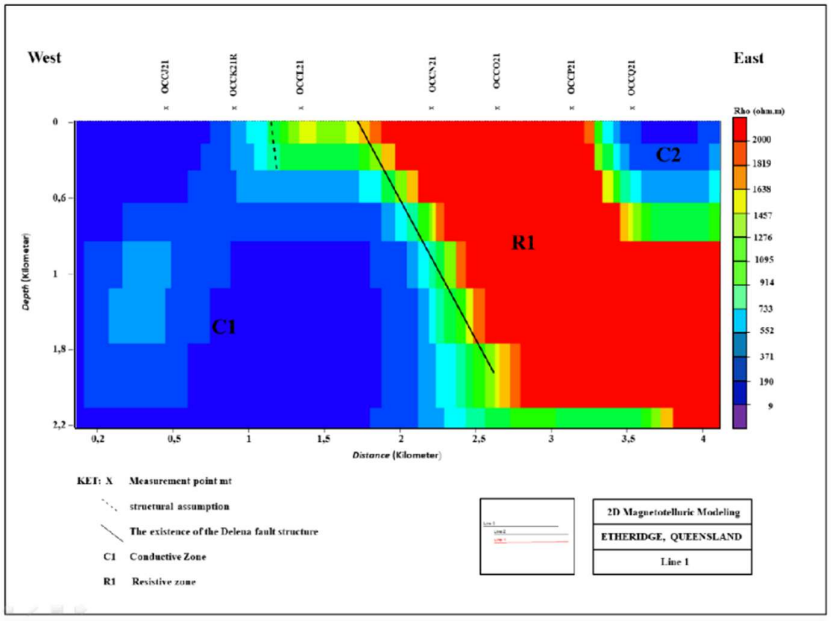

Figure 11. Results of 2D inversion modeling of line 1.

4.5. Line 2

2D modeling of Line 2 (8 stations, 450 km, 2.2 km depth) was used to estimate the northwest–southeast-trending Palmerville Structure. Inversion with parameters α0.2, β1, τ7 yielded an RMS of 4.25% and a resistivity of 9–2000 Ωm (**Figure 12**). The resistivity cross-section shows four zones: C1 (<100 Ωm, Wayaba Formation/T3 clay), light blue (100–500 Ωm, water-saturated sandstone), green (500–1500 Ωm, Loafers/Si Formation quartz), and R1 (>1500 Ωm, Kennedy Province granite) (Kirkby et al., 2020).

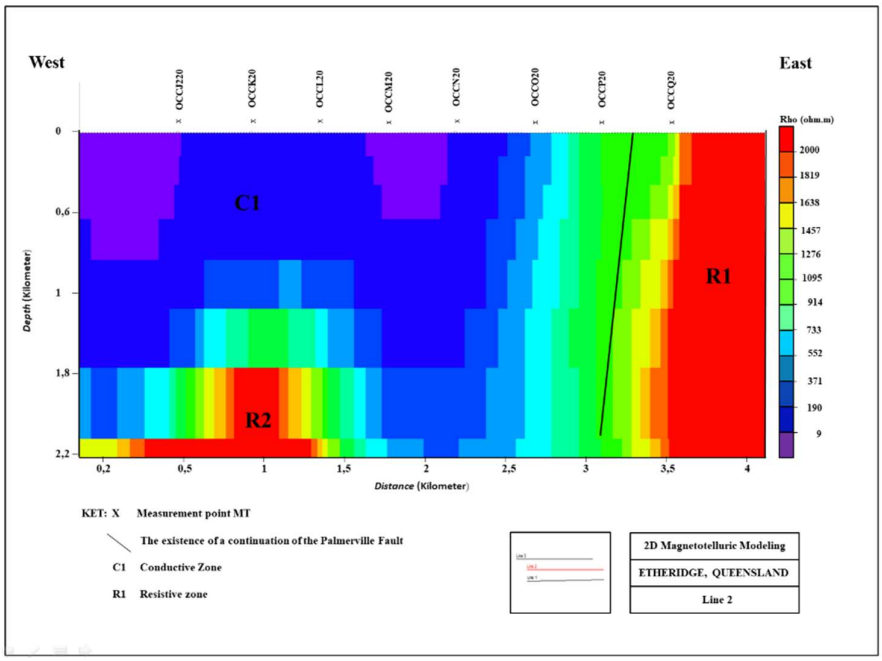

Figure 12. 2D inversion modeling results of line 2.

The results on line 2 show an increase in high resistivity (R1), which is suspected to be a fault. The C1 conductive layer continues to spread eastward to a depth of 2 kilometers. The suspected fault structure is identified in the layer between C1 and R1 because it can be assessed from the contrast direction and very low to very high resistivity values. At the OCCP20 measurement point, there is a fault confirmed as a continuation of the Palmerville Structure fault with the interpretation results of the cross-section results ensuring a depth of up to 2,200 meters, this assumption can be assured by adjusting the resistivity contrast and regional geological maps. Based on the range of resistivity values in **Table 3**, line 2 passes through 5 rock formations: Wayaba Formation (T3), Alluvium Formation (Qd), Bulimba Formation (T1), Grandiorite Loafers Formation (Si), and Kennedy Province Formation – Carboniferous Intrusive Rocks (CPg).

4.6. Line 3

2D modeling on Line 3 (West–East), involving 6 MT stations (OCCI19, OCCJ19, OCCL19, OCCN19, OCCO19, and OCCP19) along 450 km to a depth of 2.2 km, aims to detect the Palmerville Fault, which is estimated to cut in the Northwest–Southeast direction. The results of 2D inversion (using parameters *α0.5, β1, τ7*) produce a resistivity distribution of 9–2000 Ωm with an RMS error of 5.73148% (**Figure 13**), where this cross section shows four main zones: C1 (<100 Ωm, water-saturated clay from the Alluvium/Qd Formation) which is suspected to be the fault location; 100–500 Ωm zone (water-saturated sandstone); 500–1500 Ωm zone (quartz of the Gilbert River/JK Formation); and R1 (>1500 Ωm, basal Elizabeth River Formation/cpi) (Kirkby et al., 2020).

The results on line 3 show an increase in high resistivity values (R1), which are suspected to be faults. The conductive layer C1 continues to spread south to a depth of 2.2 kilometers. The suspected fault structure was identified in the R1 layer because it can be assessed from the contrast and very high resistivity values. At the OCCP19 measurement station, the presence of a fault, namely the Palmerville Structure fault which can be assumed to reach a depth of more than 2,200 meters, is suspected due to differences in resistivity values and is supported by regional geological maps. Based on the range of resistivity values in **Table 3**, line 3 passes through 5 rock formations, namely the Alluvium Formation (Qd), Wayaba Formation (T3), Claravile Formation (T2), Gilbert River Formation (JK), and Elizabeth River Formation (cpi).

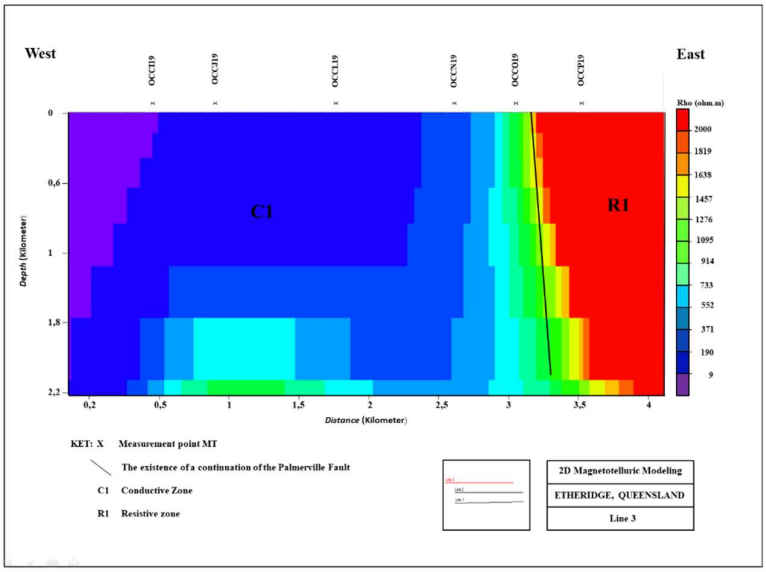

Figure 13. Results of 2D inversion modeling of line 3.

5. CONCLUSION

2D magnetotelluric (MT) modeling on Line 1, Line 2, and Line 3 successfully identified subsurface structures down to a depth of 2.2 km, including the Delaney Fault on Line 1, the Palmerville Fault on Line 2 and 3, as well as minor faults and conductive zones associated with water-saturated clay and sandstone formations, where resistivity contrasts are key indicators for interpreting faults and lithological variations. These findings have geological implications. significant, indicating the continuity of regional faults to the middle–lower crust and the relationship between fault structures and local rock formations, which helps understand tectonic patterns and potential weak zones for fluid flow or geologic stability. However, this study has limitations, including low resistivity ambiguities that could be caused by lithology or faults, limited resolution due to the distance between MT stations, and 2D assumptions that do not fully capture the 3D complexity of the subsurface media. Therefore, recommendations for future research are to conduct 3D modeling, integrate additional geophysical data such as seismic or gravity for validation, and reduce the distance between MT stations to increase resolution and reduce ambiguity in fault and lithology interpretation.

ACKNOWLEDGEMENT

The authors declare that there is no conflict of interest regarding the publication of this paper. This research received no specific grant from any funding agency in the public, commercial, or not-for-profit sectors. All authors have contributed to the preparation of this manuscript and have approved the final version.

REFERENCES

Jiang, W., Korsch, R. J., Doublier, M. P., Duan, J. (2020). Mapping Deep Electrical Conductivity Structure in The Mount Isa Region, Northern Australia: Implications for Mineral Prospectivity. *Journal of Geophysical Research: Solid Earth*. https://doi.org/10.1029/2019JB017528

Kirkby, A. L., Musgrave, R. J., Czarnota, K., Doublier, M. P., Duan, J., Cayley, R. A., & Kyi, D. (2020). Lithospheric Architecture of a Phanerozoic Orogen from Magnetotellurics: AusLAMP in The Tasmanides, Southeast Australia. *Tectonophysics*, 793, 228560. https://doi.org/10.1016/j.tecto.2020.228560

Korsch, R. J., Huston, D. L., Henderson, R. A., Blewett, R. S., Withnall, I. W., Fergusson, C. L., & Costelloe, R. D. (2012). Crustal Architecture and Geodynamics of North Queensland, Australia: Insights from Deep Seismic Reflection Profiling. *Tectonophysics*, 76-99. https://doi.org/10.1016/j.tecto.2012.02.022

Maharani, L., Paembonan, A. Y., & Irawati, S. M. (2023). Analisis Dimensionalitas Dengan Tensor Fase dan Model 2D Sistem Geotermal. *Jurnal Geosaintek*, 9(3), 167-175. http://dx.doi.org/10.12962/25023659.v9i3.17646

Murdani & Sarkowi, M. (2019). Pemodelan 2 Dimensi Data Magnetotelurik Daerah Prospek Panas Bumi Lapangan JGT. *JGE (Jurnal Geofisika Eksplorasi)*, 5.5 5-6.

Ostersen, T. C. (2024). Resistivity Anomalies in The Shallow and Deep Crust Beneath West Tasmania From A Broadband Magnetotelluric 2D Transect. *Exploration Geophysics*, 55(5), 562-574. https://doi.org/10.1080/08123985.2024.2392802

Pahri, P. P. (2023). Analisis Tensor Fase dan Pemodelan 2D Data Magnetotelurik Gabbs Valley, Nevada, USA. *JGE (Jurnal Geofisika Eksplorasi)*, 9(3), 206–216. https://doi.org/10.23960/jge.v912.301

Robertson, G. T. (2020). Quality Over Quantity: on Workflow snd Model Space Exploration of 3D inversion of MT data. *Geophysical Journal International*, 223(3), 1565–1580. https://doi.org/10.1186/s40623-019-1125-4

Simpson, F., & Bahr, K. (2005). *Practical Magnetotellurics*. Cambridge: Cambridge University Press. https://doi.org/10.1017/CBO9780511614095

Terrex, P. L. (2007). *Resistivity and Conductivity Data of the Queensland Area.* Quantec Geoscience.

Tietze, K., Thiel, S., Brand, K., & Heinson, G. (2024). Comparative 3D Inversion of Magnetotelluric Phase Tensors and Impedances Reveals Electrically Anisotropic Base of Gawler Craton, South Australia. *Exploration*

Geophysics, 55(5), 575-601. https://doi.org/10.1080/08123985.2023.2281615

Tournerie, B. (2009). *Geophysical Survey Interpretation Report: Quantec SPARTAN Magnetotelluric Transects, Northern Queensland, Australia.* Quantec Geoscience Ltd.

Withnall, I. W. & Blake, P. R. (2012). *The State of Queensland Geological Survey of Queensland.* Dapartement of Natural Resources and Mines: Geological Survey of Queensland. https://geoscience.data.qld.gov.au/dataset/mr010616

Yulianti, S. R. (2020). Identifikasi Struktur Bawah Permukaan Menggunakan Metode Magnetotellurik 2D di Daerah Cekungan Bintuni Sebagai Potensi Hidrokarbon. *JGE (Jurnal Geofisika Eksplorasi)*, 4(2), 216–228. https://doi.org/10.23960/jge.v4i2.18

Zhang, H. & Nie, F. (2024). Study of The Impact of Acquisition Parameters on Fault Feature Identification Based on Magnetotelluric Modeling. *Applied Sciences, 14(21), 9720.*, 14(21), 9720. https://doi.org/10.3390/app14219720